NASA TM X-147

TECHNICAL MEMORANDUM

X-147

FRICTION AND PRESSURE DRAG OF BOUNDARY-LAYER DIVERTER

SYSTEMS AT MACH NUMBER OF 3.0

By Leonard E. Stitt and Bernhard H. Anderson

Lewis Research Center
Cleveland, Ohio

Declassified April 23, 1962

NATIONAL AERONAUTICS AND SPACE ADMINISTRATION

WASHINGTON   January 1960

NATIONAL AERONAUTICS AND SPACE ADMINISTRATION

TECHNICAL MEMORANDUM X-147

FRICTION AND PRESSURE DRAG OF BOUNDARY-LAYER DIVERTER

SYSTEMS AT MACH NUMBER OF 3.0

By Leonard E. Stitt and Bernhard H. Anderson

SUMMARY

An experimental investigation was performed at a Mach number of 3.0 to determine the friction and pressure drags of a pylon and a 20°- and a 40°-included-angle wedge diverter over a range of Reynolds number. The results indicated that the measured friction drag coefficients agreed reasonably with that predicted by flat-plate theory. The pressure drag coefficients of the 20° and 40° wedges agreed with those presented in the literature. The total drag coefficient of the pylon and the 20° wedge diverter was about 0.36, based on diverter frontal area, while the drag coefficient of the 40° wedge was about 0.47.

INTRODUCTION

The majority of the published force data on wedge type boundary-layer diverter systems treats primarily the pressure drag (refs. 1 to 3). A few measurements of skin-friction drag are reported in references 1 and 2, but they appear to be in disagreement as to magnitude. To provide additional information obviously needed in this area a study has been conducted at the Lewis Research Center to obtain the friction and pressure drag at a Mach number of 3.0 of three representative boundary-layer diverter systems, a pylon and a 20°- and a 40°-included-angle wedge. In this investigation two different scale models of each diverter system were used to obtain data over a large range of Reynolds number and to provide overlapping data at a given Reynolds number.

This study was conducted in the Lewis 10- by 10-foot supersonic wind tunnel at a Mach number of 3.0 and a range of Reynolds number from 0.50 to 2.50×10^6 per foot.

2

SYMBOLS

C_D	drag coefficient
$C_{D,f}$	friction drag coefficient
$C_{D,p}$	pressure drag coefficient
$C_{f,i}$	incompressible skin-friction coefficient
C_p	pressure coefficient, $(p_w - p_0)/q_0$
h	diverter height
L	wedge length
l	axial distance measured from splitter-plate leading edge to diverter leading edge
p	static pressure
q	dynamic pressure
Re_x	Reynolds number based on length of run
Re_s	Reynolds number based on splitter-plate length
x	axial distance
δ	boundary-layer thickness

Subscripts:

w	wedge
0	free-stream conditions

APPARATUS AND PROCEDURE

Models and Configurations

Two complete configurations were tested simultaneously; a large-scale model was mounted on the floor of the wind tunnel and a geometrically similar one-fifth scale model was mounted on the ceiling, as shown in figure 1(a). The boundary-layer diverter models were mounted on a base plate (figs. 1(a) and (b)) which was supported by force balances. Extensions were provided on the sides of the base plate to keep the end

effects to a minimum (fig. 1(a)) but were not connected to the balance. Boundary-layer buildup was provided by generator plates installed immediately ahead of the base plate (figs. 1 and 2) that were independent of the balance. Strips of number 20 Carborundum grit were placed spanwise across the generator plates to ensure a turbulent boundary layer ahead of the diverter systems. Total-pressure surveys were made of the boundary layer by two rakes located near the leading edge and two rakes near the trailing edge of each of the two base plates with the diverter systems removed.

As shown in figure 2, the diverter configurations consisted of 20°- and 40°-included-angle wedges and a pylon type diverter, each mounted on the base plate. Two diverter heights were provided to vary h/δ. A splitter plate was mounted on top of each diverter to simulate the floor of an inlet. Strips of number 20 Carborundum grit were also used on the splitter plates to provide boundary-layer transition. For each model, two splitter-plate lengths were used to vary l/δ.

Data Reduction

The total drag of the diverter system was obtained by subtracting from the measured axial force (balance reading) the sum of the following:

(1) Base drag of the splitter plate, base plate, and diverter configuration, obtained from static-pressure measurements

(2) Pressure drag of the 5° wedge on the splitter plate, obtained from theoretical two-dimensional flow considerations

(3) Friction drag on the surface of the base plate not in the "shadow" of the splitter plate

(4) Friction drag on the upper surface and sides of the splitter plate

The friction drag on the surface of the base plate (item (3)) was obtained by running a "clean" base plate and converting the measured drag to coefficient form by referencing it to the wetted area of the base plate. The measured skin-friction drag coefficients (fig. 3(a)) are compared with the turbulent skin-friction coefficient at Mach 3.0, which is shown in reference 4 to be about 61 percent of the incompressible value. A friction drag coefficient to be used in obtaining the splitter-plate tare (item (4)) was obtained by adding an estimated drag of the generator plate to the measured drag of the "clean" base plate and referencing the drag coefficient to the combined surface area of the base and generator plates. These results are compared with the Mach 3.0 turbulent skin-friction coefficient in figure 3(b).

The pressure drag of the diverters was obtained by integrating static pressures on the face of the wedge and multiplying by the diverter frontal area. Both the total drag and pressure drag for all the diverter configurations are presented herein in coefficient form, based on an area equal to the splitter plate width multiplied by the diverter height. The diverter friction drag was obtained by subtracting the pressure drag from the total drag. The diverter friction drag coefficient is presented as a function of Reynolds number and is based on the total wetted area under the splitter plate.

RESULTS AND DISCUSSION

The boundary-layer thicknesses on the base plates of the two models, with diverters removed, are presented for a range of Reynolds number in figure 4 and compared with the theoretical thicknesses for smooth flat plates. Included are data from both front and rear total-pressure rakes. Even with roughness near the leading edge of the generator plate, it appears that the boundary layer on the small model at Reynolds numbers below about 1 million was in a region of transition. The boundary-layer thickness determined on the model in reference 1 is included in figure 4. For that model the boundary layer at the lowest Reynolds number also appears to be in the transition region. A curve was faired through the experimental data (dashed line) and values of h/δ and l/δ were computed for all the configurations tested and are presented in table I over the range of test conditions.

Typical diverter pressure distributions for the three diverter configurations are presented in figure 5 for the large and small models at the same Reynolds number based on splitter-plate length. At any given station along the wedge there was very little vertical variation in static pressure. For both the 20°- and the 40°-included-angle wedge the initial pressure coefficient was higher than the theoretical two-dimensional value. The bow shock that existed ahead of the wedge was probably contained by the splitter plate, since no such shock was visible from schlieren observations. For the 20° wedge the flow expanded to near stream pressure in about 40 percent of its length, and for the 40° wedge in about 80 percent of its length. The differences in pressure coefficient between the large- and small-scale models could have resulted from the differences in h/δ and l/δ that are indicated at the top of the figure, since the data were obtained at the same Reynolds number.

The pressure and total drag coefficients for all the configurations are presented in figure 6 over a range of Reynolds number based on splitter-plate length. The drag coefficient is referenced to an area equal to the splitter-plate width times the diverter height. Values of h/δ and l/δ are presented in table I, since these parameters vary with Reynolds number. The decrease in total drag coefficient at Reynolds

numbers below about 3 million resulted from the laminar flow on the small model, as discussed in connection with figure 4. The pressure drag was only a small part of the total drag of the pylon model and was the larger part of the total drag for the 40°-included-angle wedge. The total drag coefficient of the 20° wedge was about the same as for the pylon, that is, about 0.36 based on frontal area, while the drag coefficient of the 40° wedge was about 0.47.

The wedge pressure drag coefficients obtained in the present investigation appear to be in general agreement with those obtained in references 1 to 3, as shown in figure 7. Data obtained from the other sources are presented as shaded symbols. The theoretical Mach 3.0 two-dimensional pressure coefficient is also included for comparison purposes.

The main object of this investigation was to obtain the friction drag coefficient as a function of Reynolds number. The skin-friction drag coefficient was obtained by subtracting the pressure drag coefficient from the total drag coefficient in figure 6 and changing the reference area to wetted area. In this investigation the wetted area includes all surfaces between the splitter plate and the base plate that would be in the "shadow" of the splitter plate. The skin-friction drag coefficient is presented in figure 8 for each of the three diverter configurations without regard to variations in h/δ and l/δ. These drag coefficients are compared with the Mach 3.0 flat-plate turbulent skin-friction coefficient, which, as mentioned before, is about 61 percent of the incompressible value. The data are presented over a range of Reynolds number, based on splitter-plate length, and indicate that the theoretical curve $\left(C_{D,f} = 0.61\ C_{f,i}\right)$ may be adequate in the design of boundary-layer diverter systems of this type.

The skin-friction drag coefficients obtained at low Reynolds numbers in the present program agree with the single value of 0.003, presented in reference 2, which was also obtained at a low value of Reynolds number. The skin-friction drag coefficients computed from wake total-pressure surveys in reference 1 were higher than those obtained in the present tests. For example, skin-friction drag coefficients from reference 1 ranged from 0.008 at a Reynolds number of 1.3×10^6 to 0.023 at a Reynolds number of 0.65×10^6. These higher values might possibly be a direct result of the wake survey method of obtaining skin friction. However, it should be noted that in the low Reynolds number range of these small tunnel models (less than 1.0×10^6) a slight decrease in Reynolds number has a very large effect on skin-friction coefficient, as can be seen in figure 8.

SUMMARY OF RESULTS

The following results were obtained at Mach 3 for three boundary-layer diverter systems, a pylon, a 20°-, and a 40°-included-angle wedge:

1. The measured skin-friction drag coefficient over a range of Reynolds number agreed fairly well with that predicted by compressible flat-plate theory.

2. The measured pressure drag coefficients for the 20°- and 40°-included-angle wedge diverters agreed with those presented in the literature.

3. The measured drag coefficient of the pylon and the 20° wedge diverter was about 0.36 based on frontal area, while the drag coefficient of the 40° wedge was about 0.47.

Lewis Research Center
　　National Aeronautics and Space Administration
　　　　Cleveland, Ohio, September 30, 1959

REFERENCES

1. Piercy, Thomas G., and Johnson, Harry W.: Experimental Investigation at Mach Numbers 1.88, 3.16, and 3.83 of Pressure Drag of Wedge Diverters Simulating Boundary-Layer-Removal Systems for Side Inlets. NACA RM E53L14b, 1954.

2. McLafferty, G. H., et al.: Investigation of Turbojet Inlet Design Parameters. R-0790-13, United Aircraft Corp., Dec. 1955. (Contract NOas 55-133-c.)

3. Campbell, Robert C., and Kremzier, Emil J.: Performance of Wedge-Type Boundary-Layer Diverters for Side Inlets at Supersonic Speeds. NACA RM E54C23, 1954.

4. Wilson, Robert E.: Turbulent Boundary-Layer Characteristics at Supersonic Speeds - Theory and Experiment. Jour. Aero. Sci., vol. 17, no. 9, Sept. 1950, pp. 585-594.

TABLE I. - BOUNDARY-LAYER CHARACTERISTICS

| Re/ft $\times 10^{-6}$	Re$_x$ $\times 10^{-6}$	Re$_S$ $\times 10^{-6}$	δ, in.	$1/\delta$	h/δ	
					h = 1.00 in.	h = 1.25 in.
Large model - short splitter plate						
0.50	2.92	5.0	1.27	4.9	0.79	0.99
.75	4.4	7.5	1.20	5.2	.83	1.04
1.00	5.85	9.9	1.14	5.5	.88	1.10
1.50	8.8	14.9	1.07	5.8	.94	1.17
2.00	11.7	19.9	1.03	6.1	.97	1.21
2.50	14.6	24.8	1.00	6.3	1.00	1.25
Large model - long splitter plate						
0.50	2.66	5.2	1.18	10.6	0.85	1.06
.75	3.98	7.8	1.10	11.4	.91	1.14
1.00	5.31	10.5	1.06	11.8	.94	1.18
1.50	7.98	15.7	.99	12.6	1.01	1.26
2.00	10.60	20.9	.95	13.2	1.05	1.32
2.50	13.30	26.2	.92	13.6	1.09	1.36
Re/ft $\times 10^{-6}$	Re$_x$ $\times 10^{-6}$	Re$_S$ $\times 10^{-6}$	δ, in.	$1/\delta$	h/δ	
					h = 0.20 in.	h = 0.25 in.
Small model - short splitter plate						
0.50	0.46	0.99	0.144	8.70	1.39	1.74
.75	.69	1.49	.140	8.93	1.43	1.78
1.00	.92	1.98	.145	8.60	1.38	1.72
1.50	1.38	2.98	.176	7.10	1.14	1.42
2.00	1.84	3.97	.191	6.55	1.05	1.31
2.50	2.30	4.96	.198	6.3	1.01	1.26
Small model - long splitter plate						
0.50	0.41	1.05	0.130	19.2	1.54	1.92
.75	.61	1.57	.124	20.2	1.61	2.02
1.00	.82	2.09	.125	20.0	1.60	2.00
1.50	1.22	3.13	.146	17.1	1.37	1.71
2.00	1.63	4.18	.165	15.1	1.21	1.51
2.50	2.04	5.23	.174	14.4	1.15	1.44

8
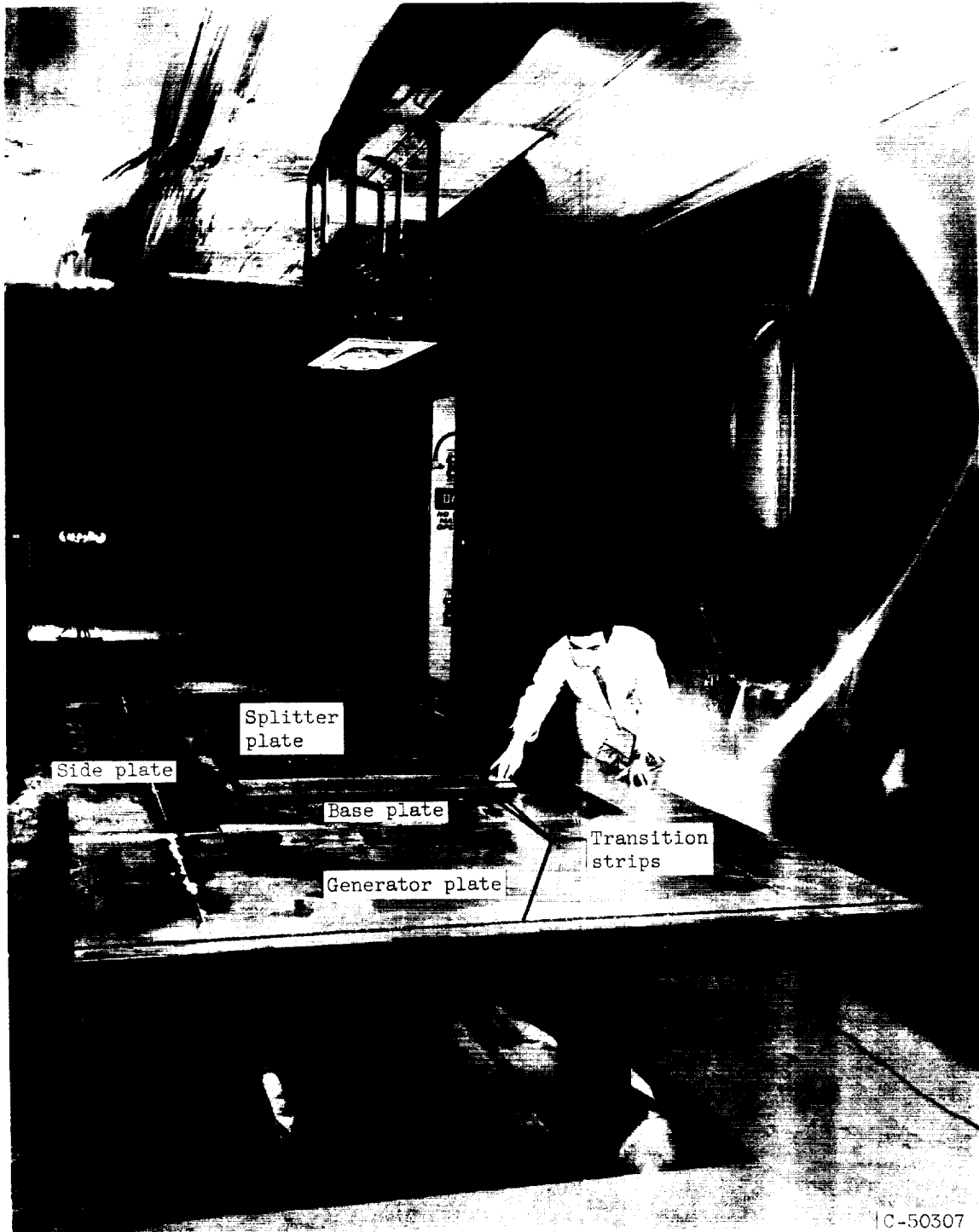
(a) General view.

Figure 1. - Boundary-layer diverter models mounted in 10- by 10-foot supersonic wind tunnel.
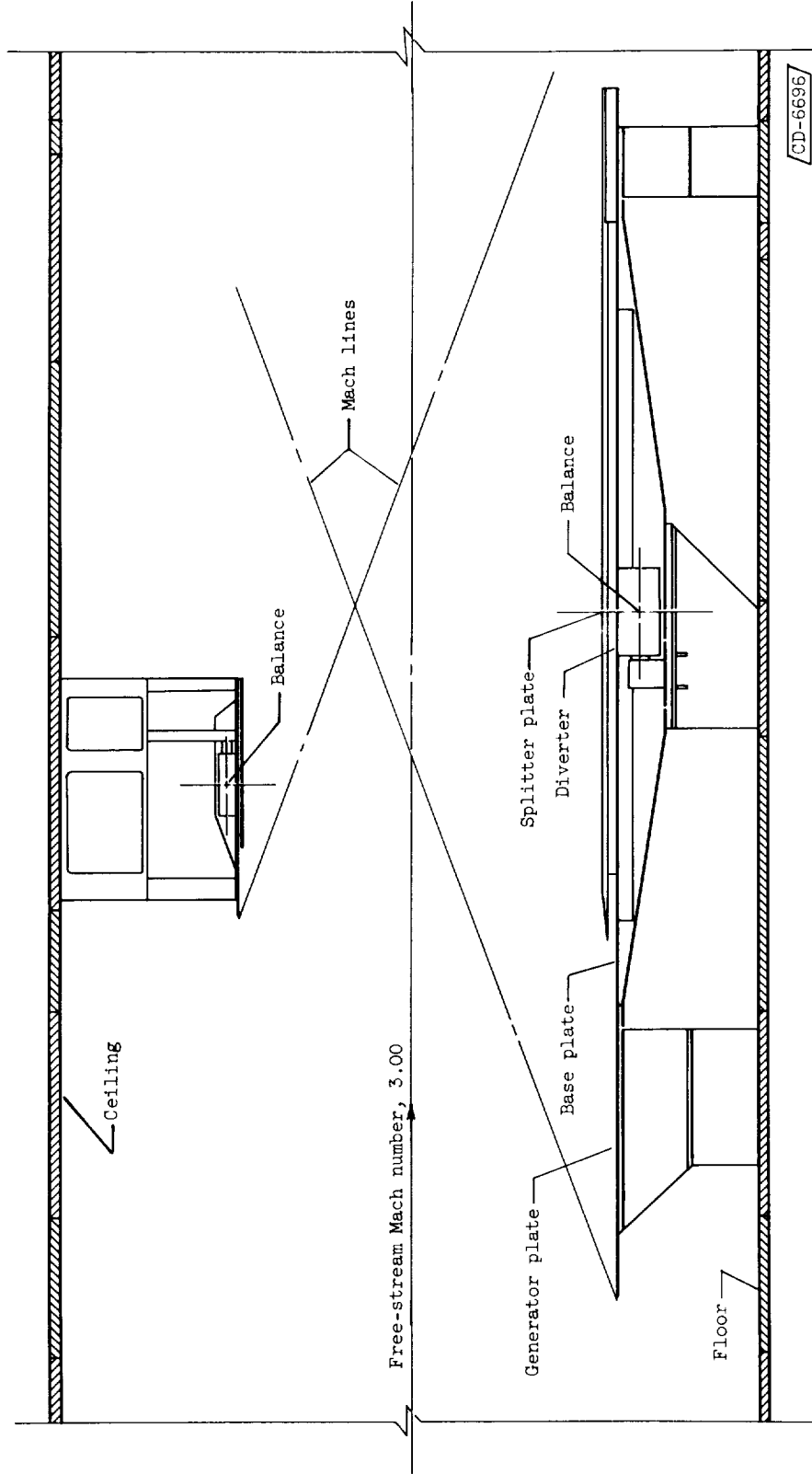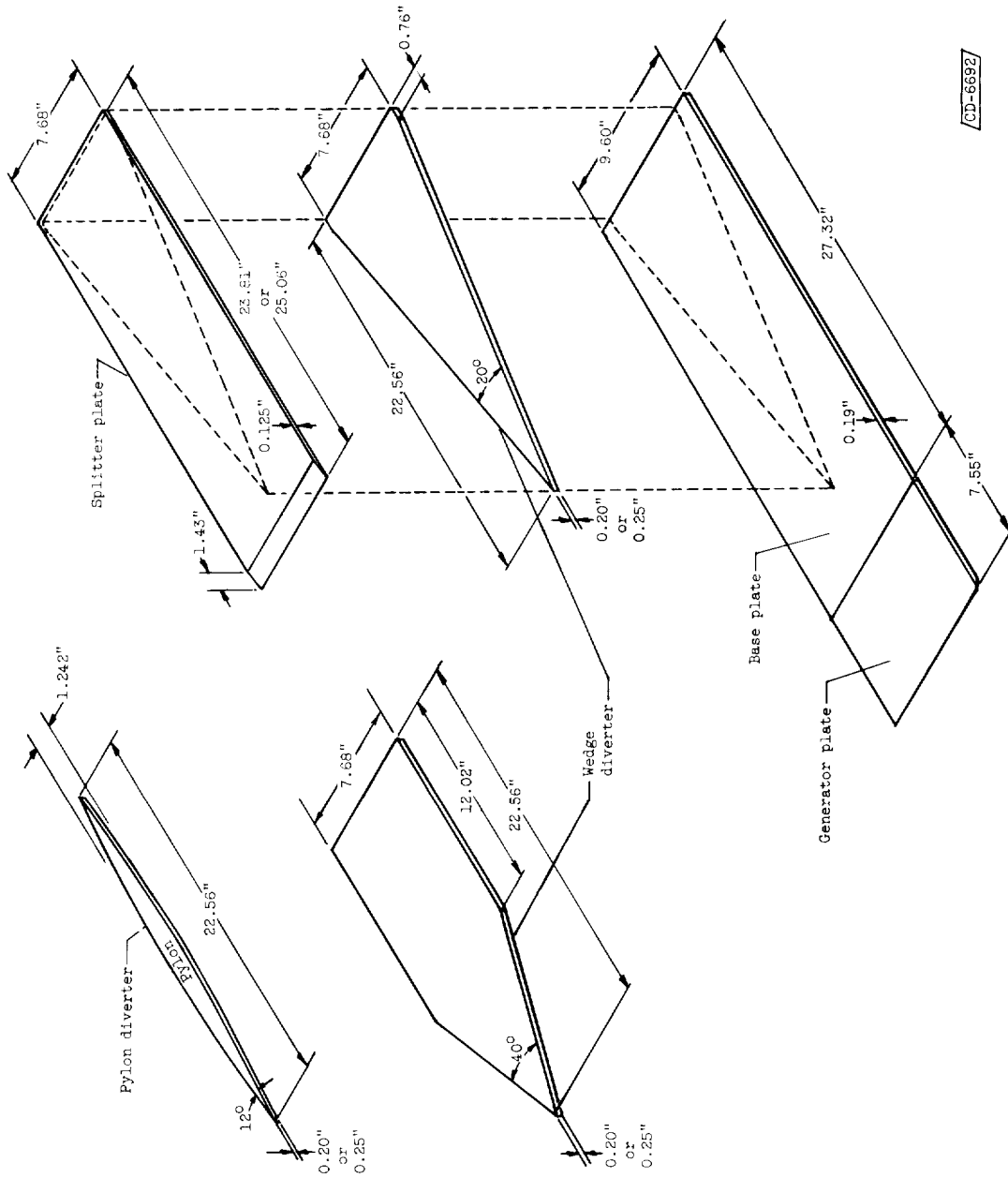
Figure 1. - Concluded. Boundary-layer diverter models mounted in 10- by 10-foot supersonic wind tunnel.

(b) Side view.
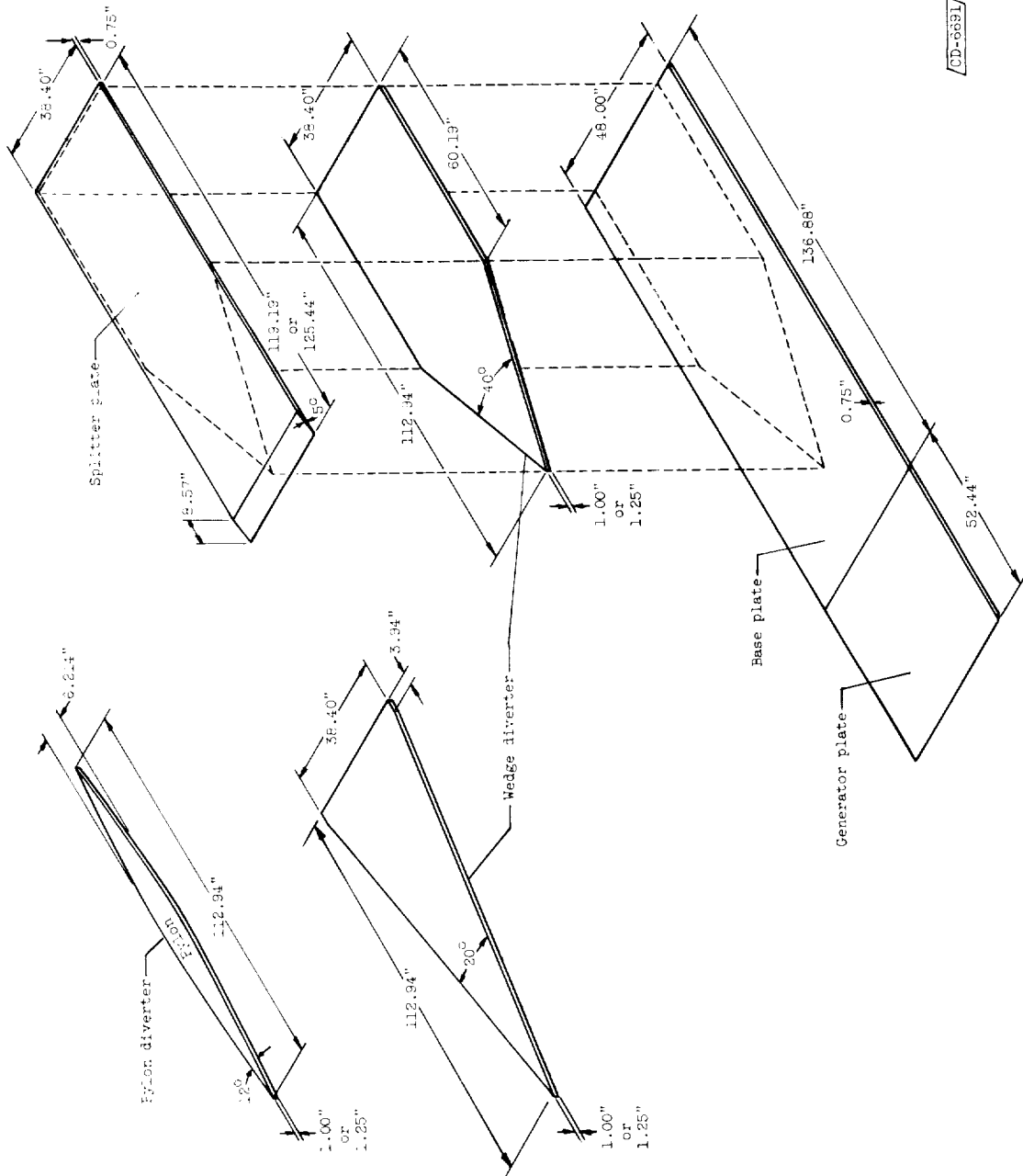
(a) Large model.

Figure 2. - Boundary-layer diverter configurations.

CD-6691

11

(b) Small model.

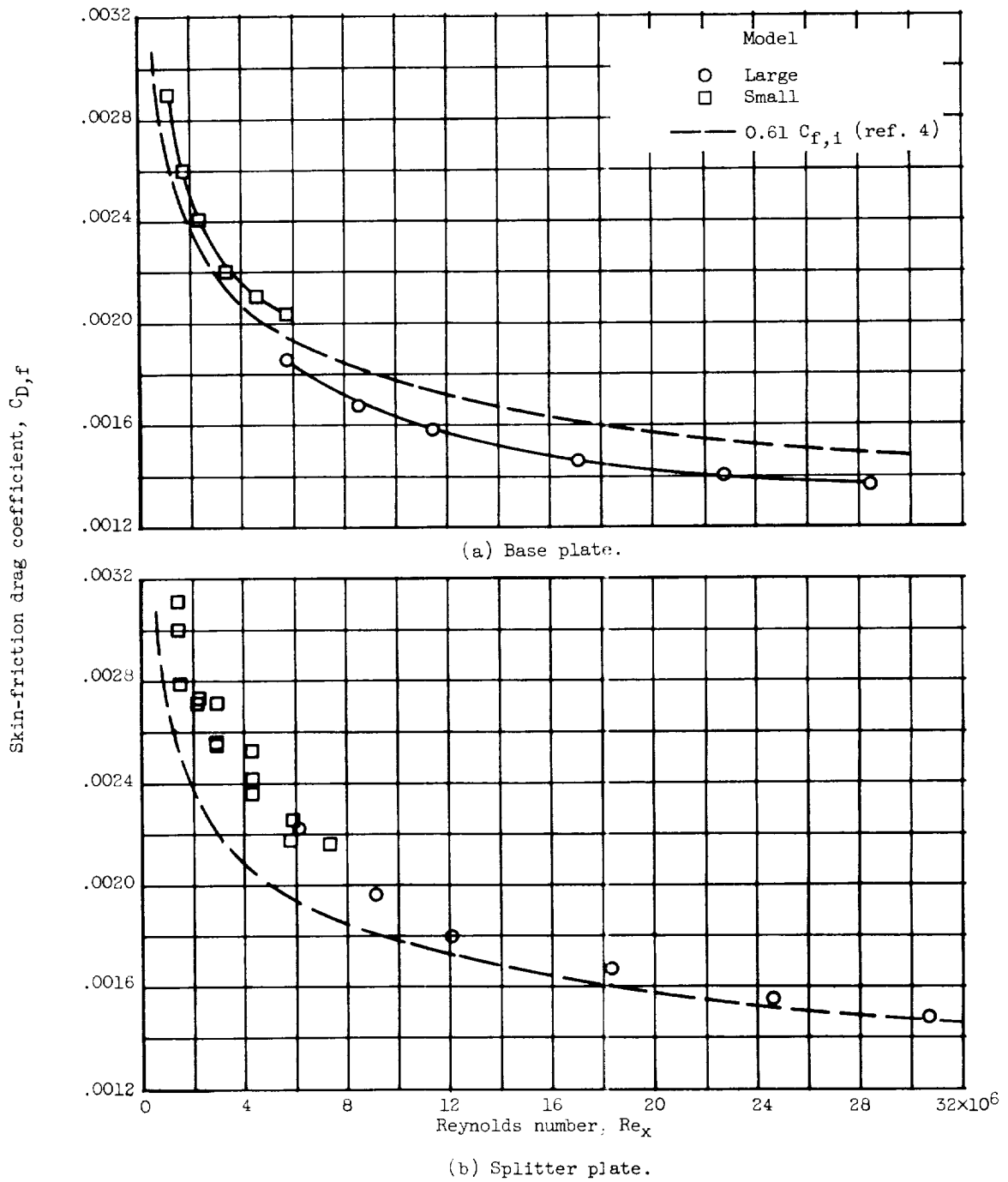Figure 2. - Concluded. Boundary-layer diverter configurations.

(a) Base plate.

(b) Splitter plate.

Figure 3. - Boundary-layer diverter models tare forces.
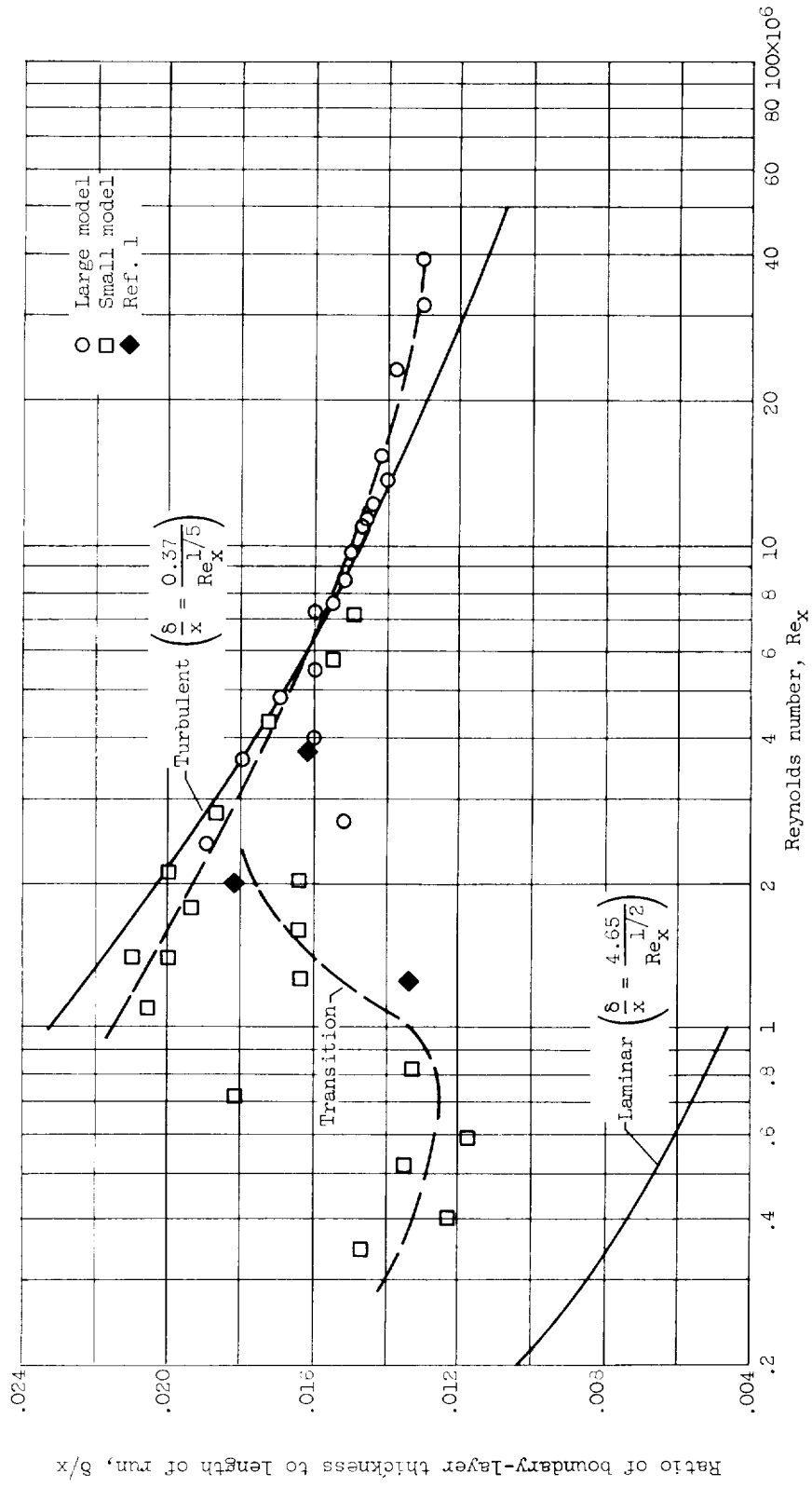
Figure 4. - Boundary-layer thickness on flat plate with roughness near leading edge.

14
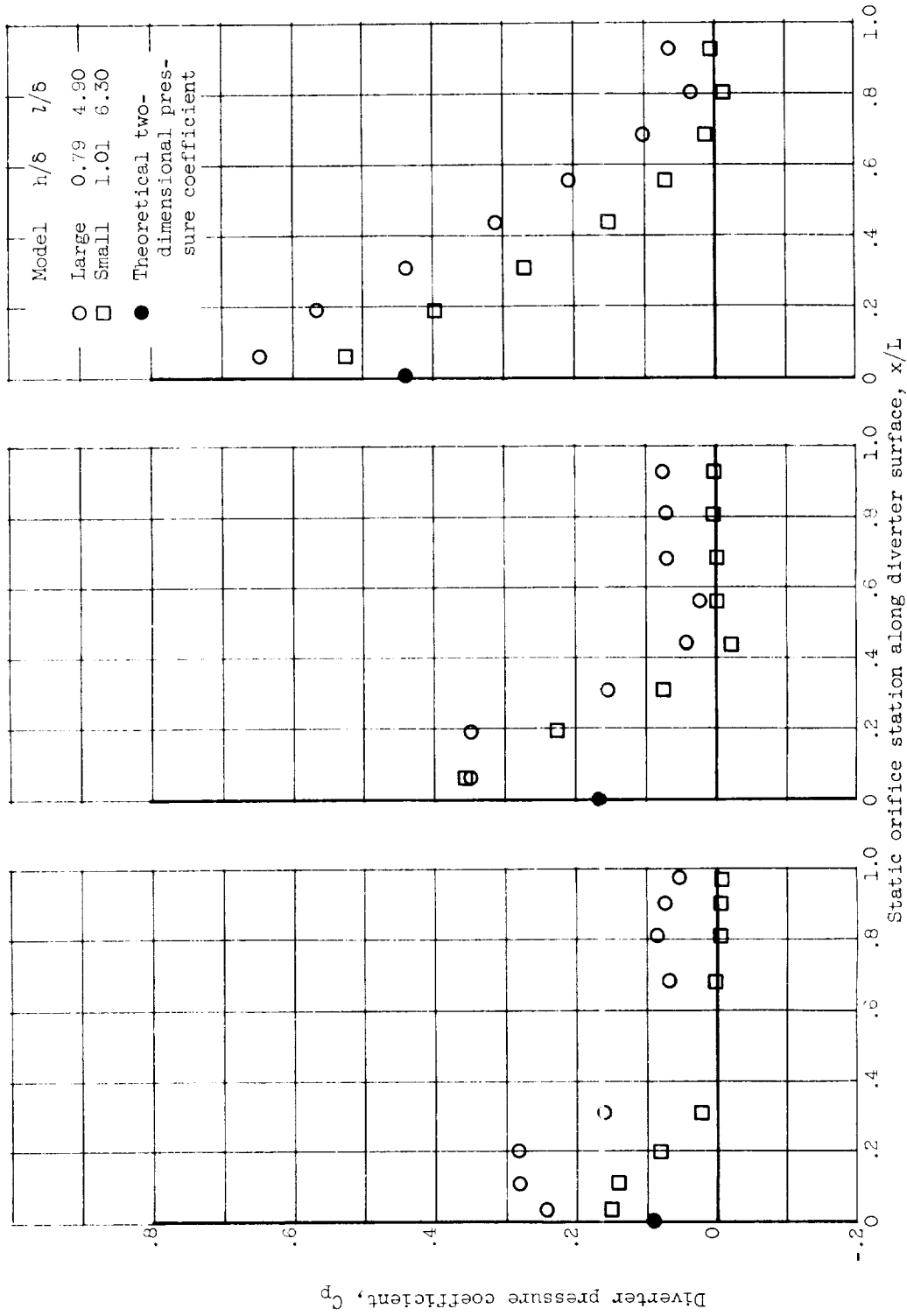
(a) Pylon models.   (b) 20°-Included-angle wedge.   (c) 40°-Included-angle wedge.

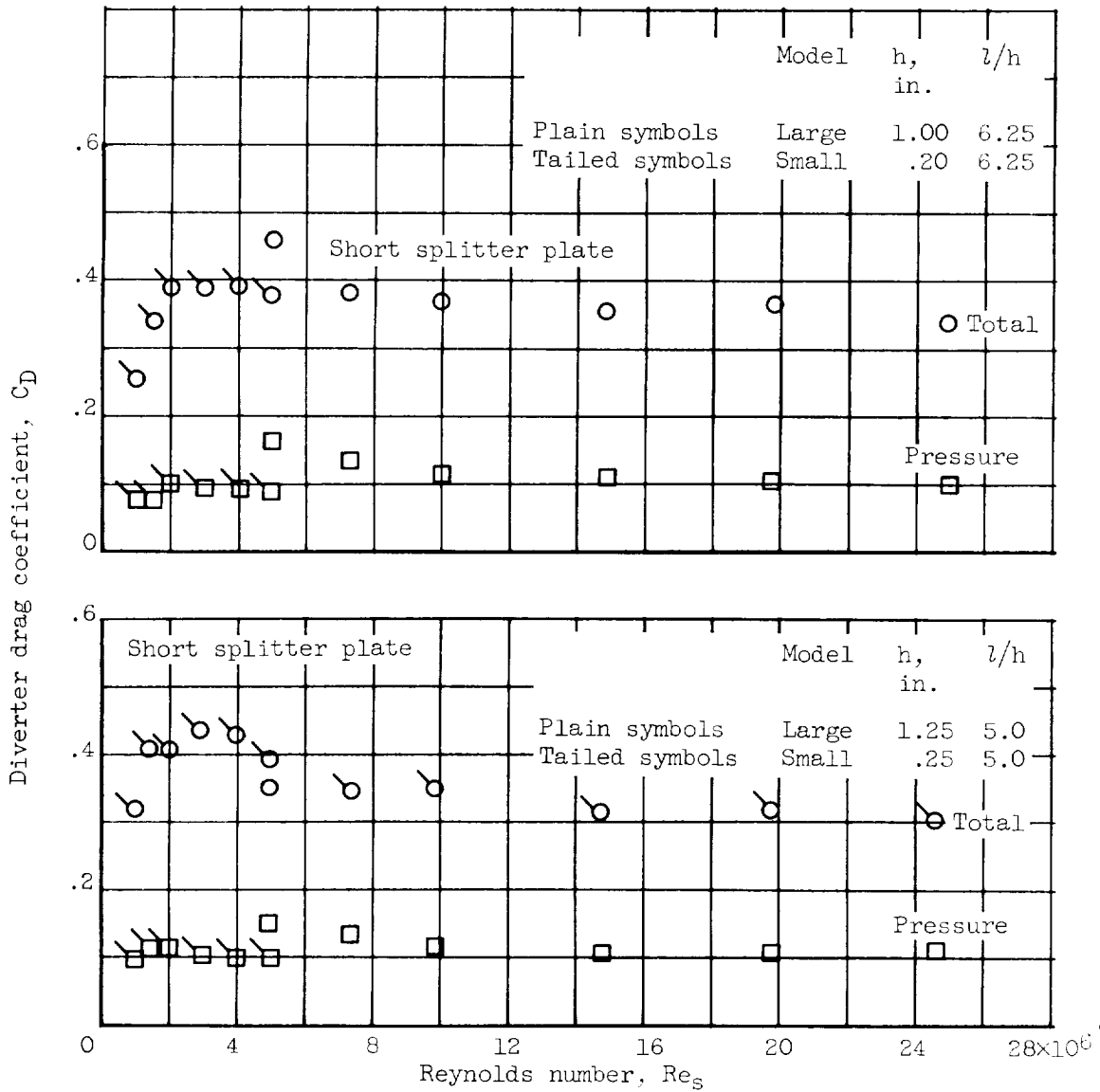Figure 5. - Boundary-layer diverter pressure distributions. Reynolds number, $Re_s \cong 5.00 \times 10^6$.
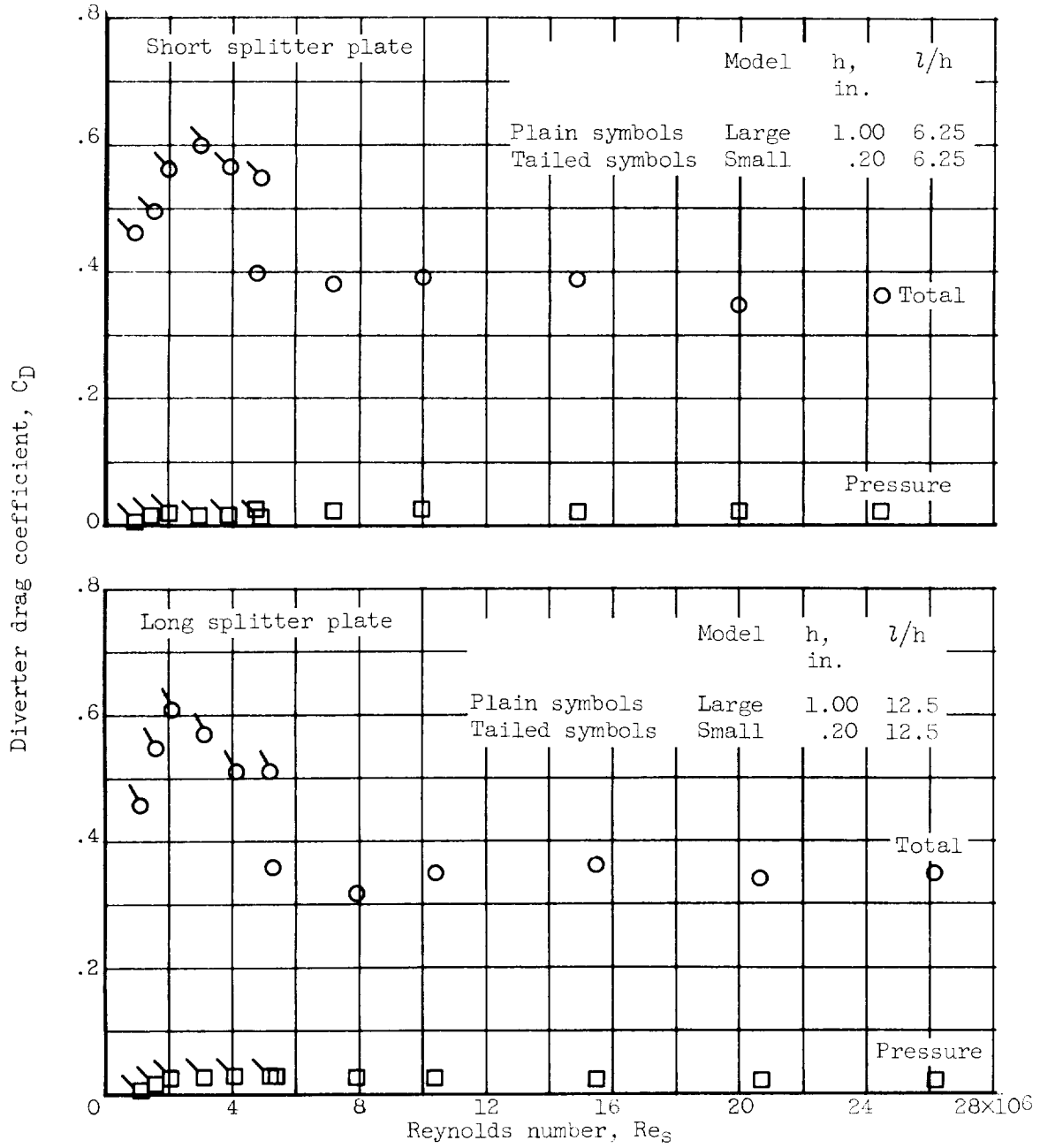
(a) Pylon models.
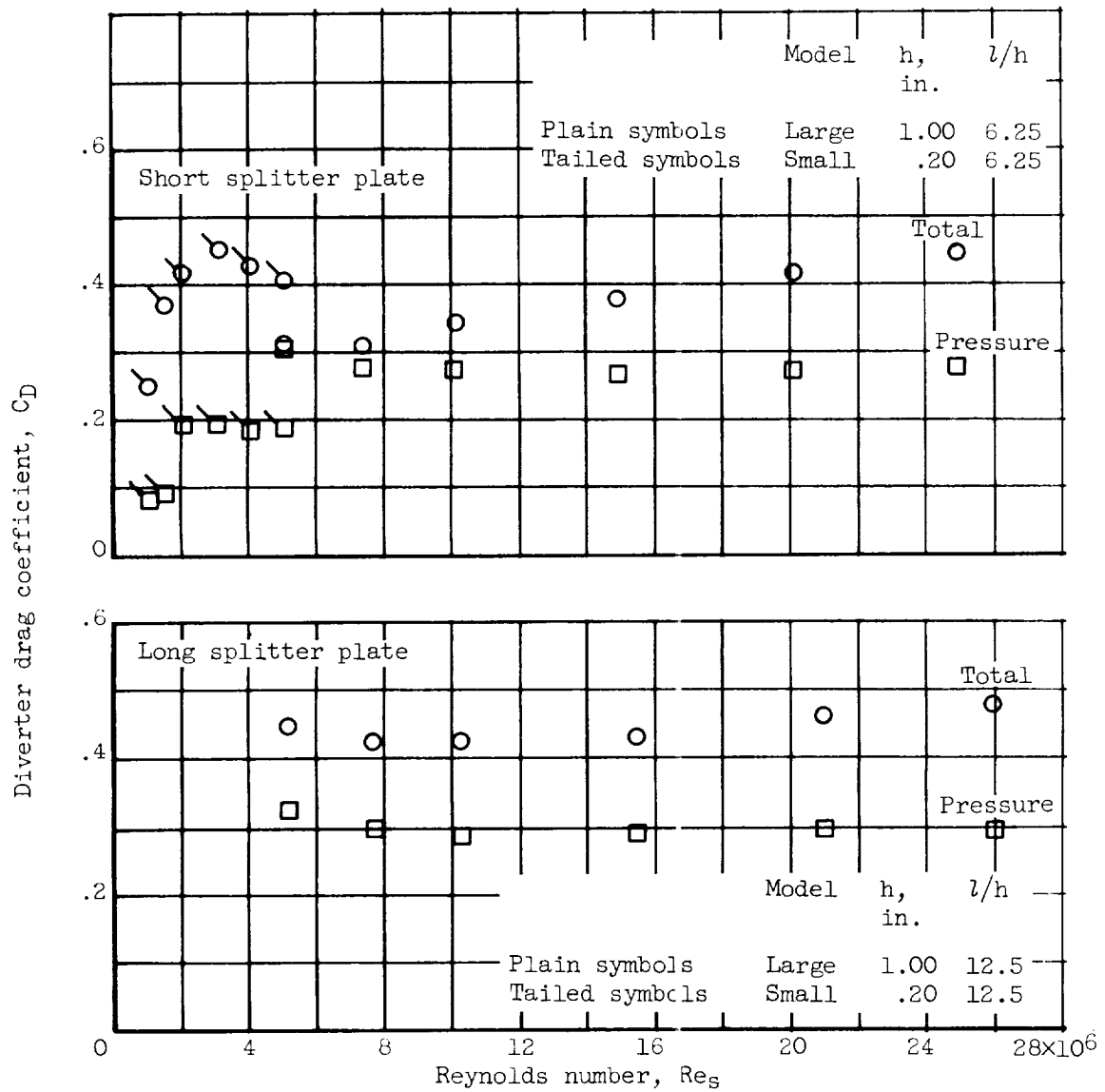
Figure 6. - Boundary-layer diverter drag.
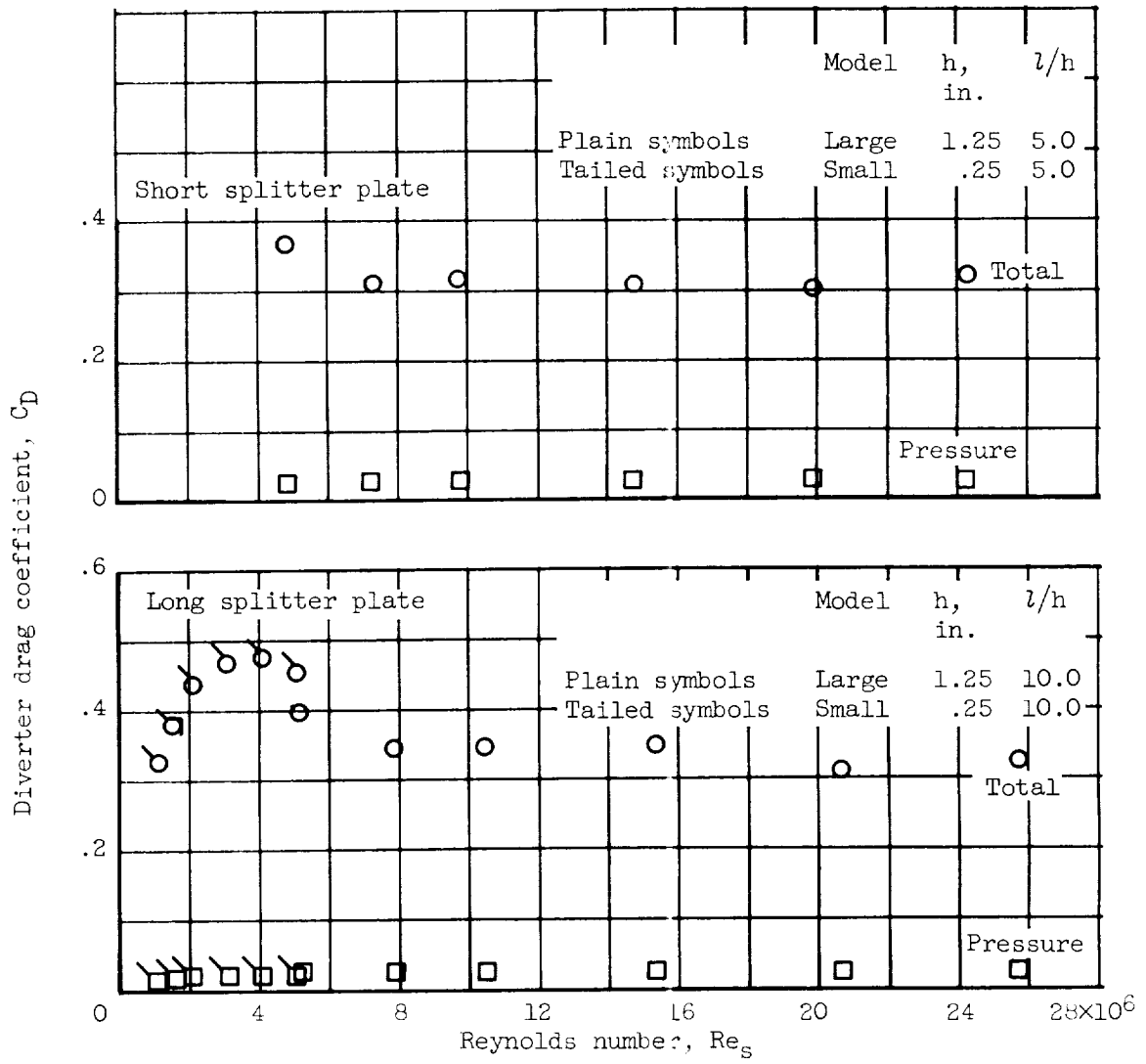
(a) Concluded. Pylon models.

Figure 6. - Continued. Boundary-layer diverter drag.

(b) 20°-Included-angle wedge.

Figure 6. - Continued. Boundary-layer diverter drag.

(c) 40°-Included-angle wedge.
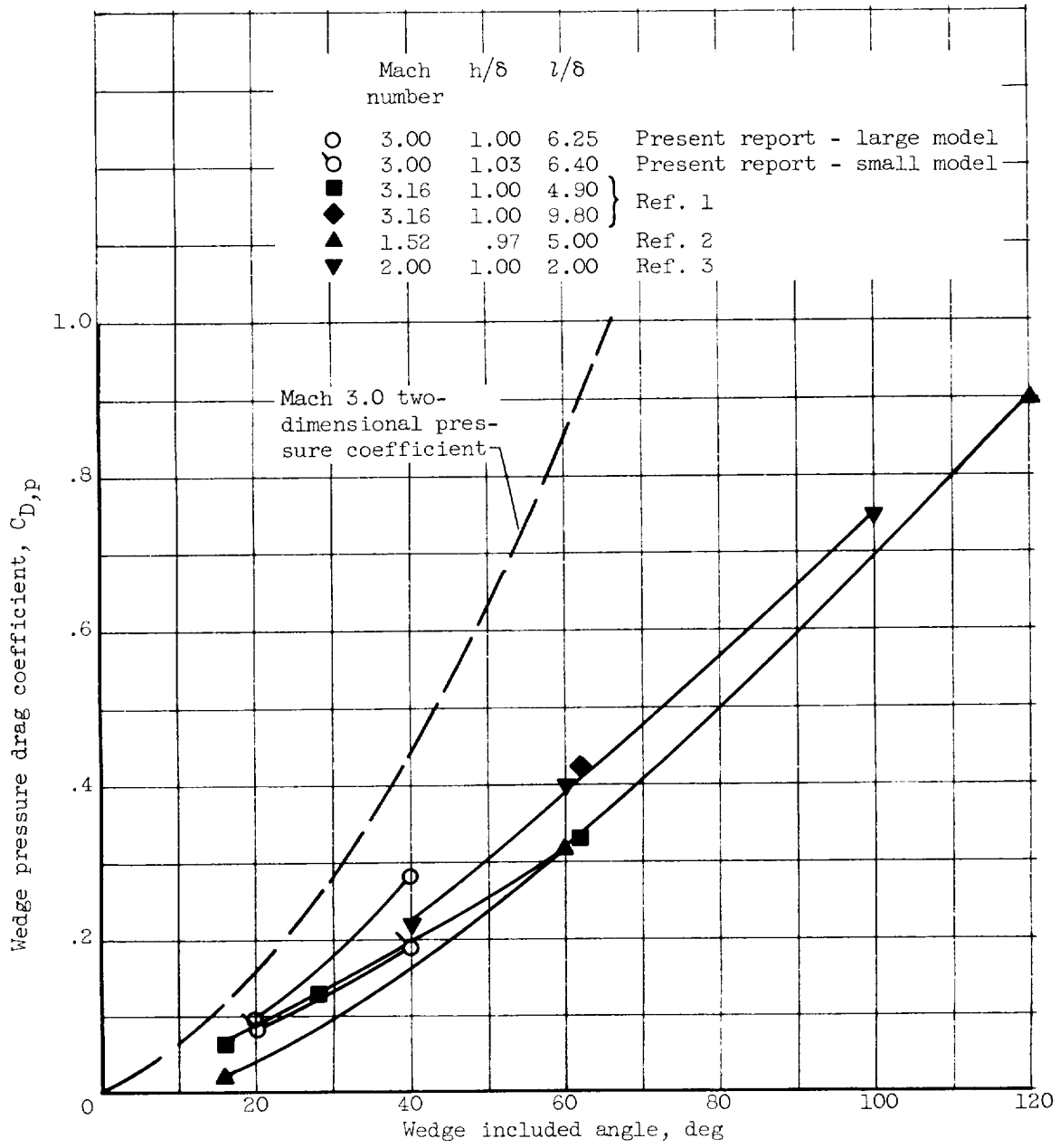
Figure 6. - Concluded. Boundary-layer diverter drag.

Figure 7. - Comparison of diverter wedge pressure drag with data from literature.

(a) Pylon models.

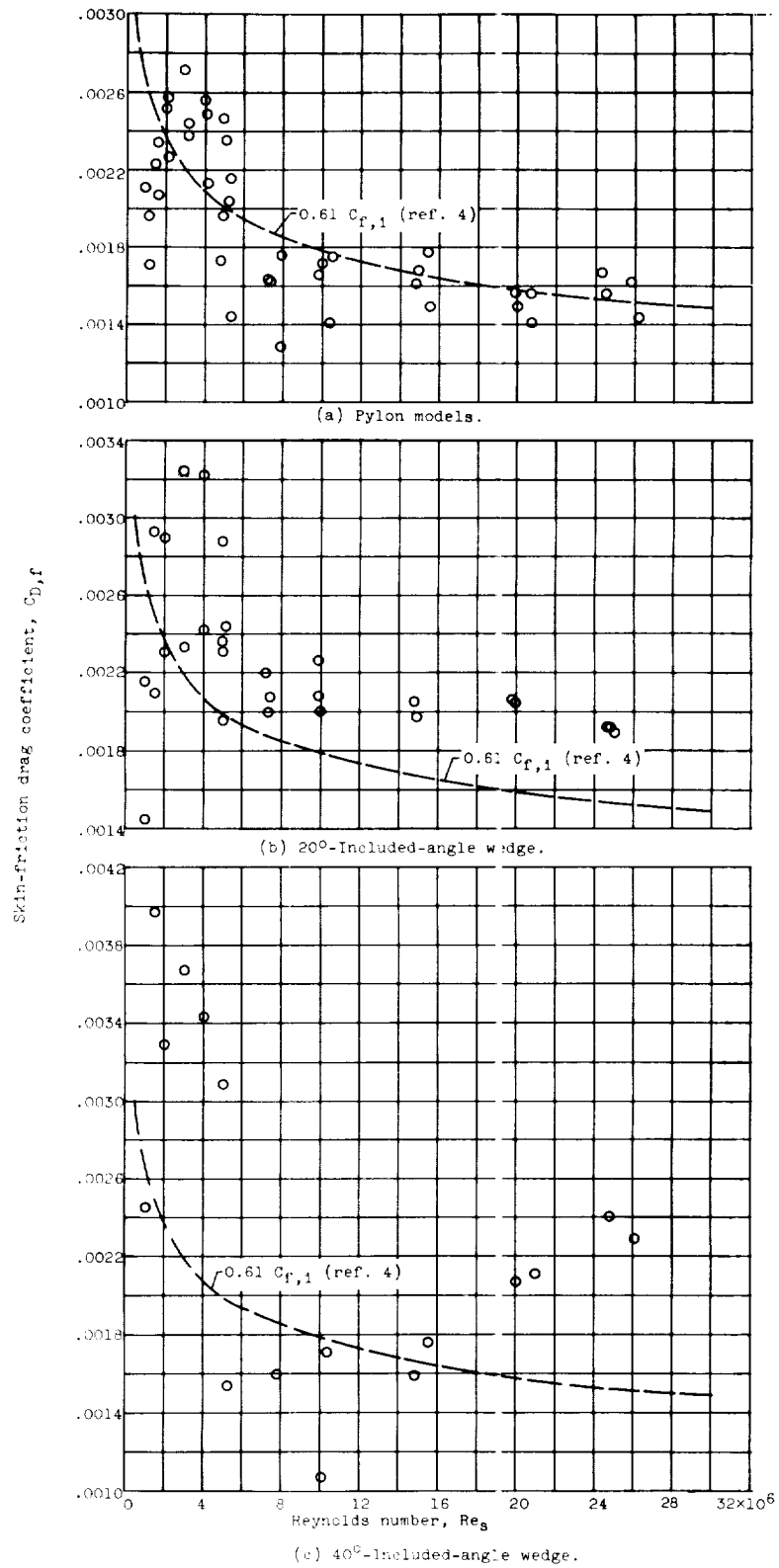(b) 20°-Included-angle wedge.

(c) 40°-Included-angle wedge.

Figure 8. - Friction drag of boundary-layer diverter models.